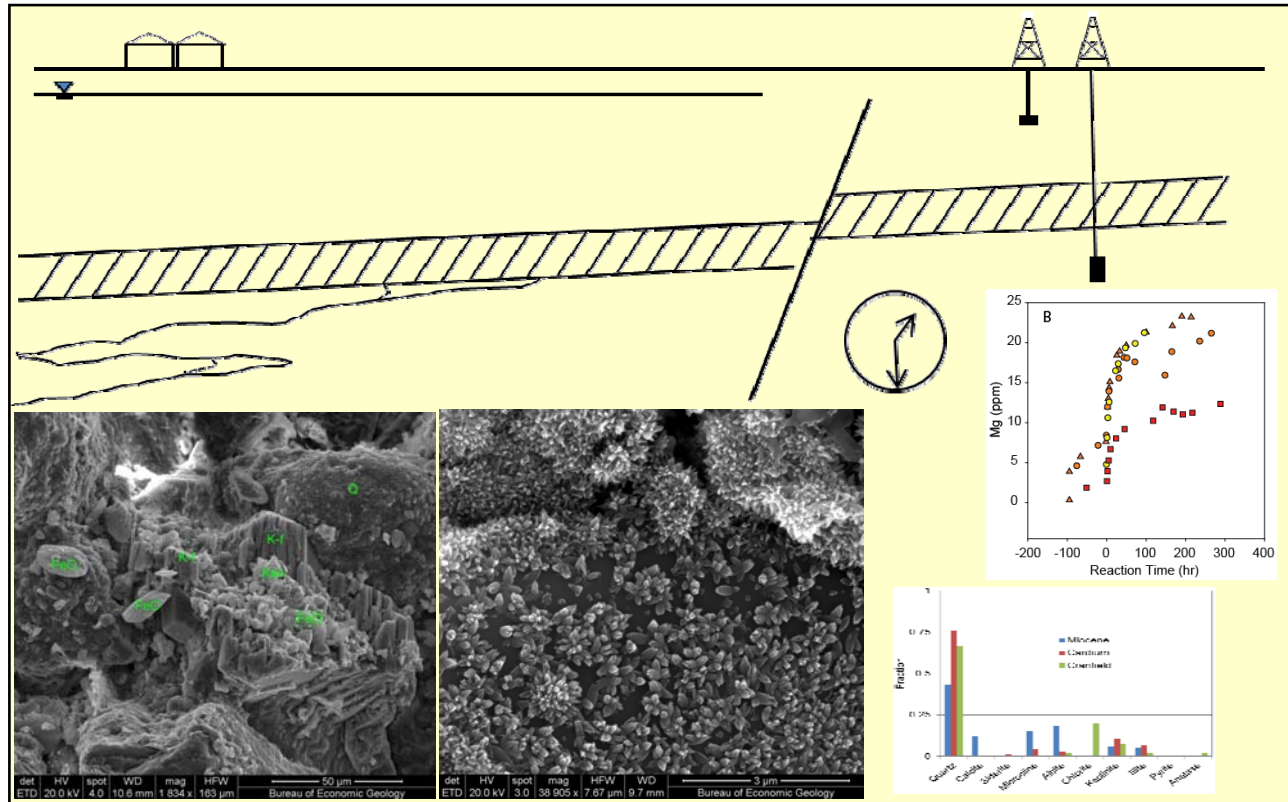


February 2013

Impact of CO₂ Impurities on Storage Performance and Assurance



**Report on Tasks 5 (Integration of Flow and Geochemistry) and Final Report
Prepared for:
CO₂ Capture Project (Phase III)**

**by
Jean-Philippe Nicot
Project Collaborators:**

S. V. Solano, J. Lu, P. Mickler, C. Yang, K. Romanak, and R. T. Johns^{*,#}

^{*}: Department of Petroleum and Geosystems Engineering, The University of Texas at Austin

[#]: now at Department of Energy and Mineral Engineering, The Pennsylvania State University

Bureau of Economic Geology
John A. and Katherine G. Jackson School of Geosciences
The University of Texas at Austin
Austin, Texas 78713-8924

**Impact of CO₂ Impurities
on Storage Performance and Assurance**
Tasks 5: Integration of Flow and Geochemistry and Final Report

Jean-Philippe Nicot,
Project Collaborators:
S. V. Solano, J. Lu, P. Mickler, C. Yang, K. Romanak, and R. T. Johns

Bureau of Economic Geology
John A. and Katherine G. Jackson School of Geosciences
The University of Texas at Austin
Austin, Texas 78713-8924

Executive Summary

A key impediment to carbon capture and storage is the cost of CO₂ capture, particularly for conventional power plants whose flue gas is dominated by gases other than CO₂. Waste-gas streams from power plants that use novel technologies (such as oxyfuel, the focus of this work) can circumvent the capture step thanks to their CO₂-rich composition (CO₂>90%), but at the expense of stream CO₂ purity. In addition to CO₂, two no-reactive gas make the bulk of impurities N₂ and Ar. O₂ is the reactive gas the most commonly cited with molar concentration ranging from <1% to >5%. Other minor species may also be present. Relatively high purity levels must be achieved to avoid compression and complications in pipeline transportation (two-phase flow) and, potentially, subsurface impacts. This work investigates the latter, which, in turn, informs techno-economic assessments of capture and transportation economics. Subsurface impacts of an impure CO₂ stream could be twofold: (1) complicate flow behavior and reduce static capacity because of density and viscosity differences and (2) undermine reservoir and top seal integrity due to reaction with reactive species (O₂, CO, SO_x).

Using a range of potential oxyfuel waste-gas compositions, we approached the first issue through a desktop study using the numerical modeling tool. So that we could work with accurate flow parameters, we performed laboratory experiments in order to determine the actual viscosity and density of the mixtures. Information on solubility of these various mixture components in the aqueous phase under various pressure, temperature, and salinity conditions was also collected. An important observation controlling all study results was that viscosity and density of the mixtures considered are lower than those of pure CO₂ at the same temperatures and pressures. It follows that a plume of CO₂ with impurities, moving updip with no barrier, will therefore migrate farther from the point of injection but will be trapped through residual saturation sooner than will a plume of pure CO₂ and possibly enhance dissolution, primarily because it is exposed to more rock / brine volume. A larger plume, however, means that a larger area must be defined and monitored for leakage pathways, such as faults and wells, but the faster trapping translates into a shorter monitoring period. Equally important is that contrasts of viscosity and density between pure CO₂ and a CO₂ mixture decrease with depth, suggesting that differences in flow behavior and storage capacity are proportionally reduced with depth.

Whereas flow behavior may impact the larger storage venue reservoir and seal rocks, geochemical impacts are more likely to be restricted to the well-bore environment and adjacent proximal reservoir. Detrimental reactions occurring close to the wellbore could be handled by established operational approaches if their origin and symptoms are understood. Batch experiments conducted in high-pressure, high-temperature autoclaves with siliciclastic (that is, quartz-rich) rocks immersed in synthetic brine and exposed to supercritical CO₂ with and without admixed O₂ show that O₂ is likely to alter the geochemistry of subsurface systems in ways that the pure CO₂ case does not, in particular when ferrous-iron bearing minerals are present. For example, pyrite (FeS₂) is quickly oxidized by O₂ and pH can drop significantly if the system has little or no buffering capacity leading to deeper degradation of feldspars (here, mostly K and Na silicate). Iron-bearing carbonates (e.g., ferroan calcite, siderite, ankerite) are degraded formation of carbonic acid with CO₂ addition. This mobilizes ferrous Fe which then precipitates as iron oxides when contacted by O₂. Iron-bearing chlorite is also mildly attacked by O₂ with subsequent iron oxide precipitation. In all 19 of the autoclave experiments runs, mineral precipitation remained minor because the precursor minerals that supply component ions are not abundant.

This suggests that as long as a precursor reactive mineral fraction is a small portion of the rock, O₂ will not have a large geochemical effect on mineral precipitation and therefore on rock stability or fluid flow.

In terms of plume shape and extent, the impact of impurities is more marked at shallow depths, where the contrast in density and viscosity with neat CO₂ is the largest. This density contrast diminishes considerably at depth. The results also suggest a trade-off between plume extent (area of review with risk of CO₂ leakage) and decreased risk owing to faster trapping. A larger plume translates into a larger area to inspect for leakage pathways, such as faults and abandoned wells, but a faster trapping translates into a shorter period of time to monitor the site. Heterogeneities seem to dampen the impact of impurities, but not in all cases. The overall results of the study may, therefore, present the CO₂ storage project developer with tradeoffs in capacity, pressure evolution, and monitoring scenarios, with additional costs likely more than offset by reduced capture costs.

Table of Contents

Executive Summary	i
Table of Contents	iii
List of Figures	iv
List of Tables	v
Acknowledgments	vi
Acronyms	vi
I. Introduction	1
II. Flow Dynamics Findings	3
II-1. Summary of Flow Dynamics Findings	3
II-2. Illustration of Key Flow Dynamics Findings	4
III. Geochemistry Findings	11
III-1. Summary of Geochemistry Findings	11
III-2. Illustration of Key Geochemical Findings	14
IV. Discussion and Conclusions	21
V. References	25

List of Figures

Figure 1. Density (a), viscosity (b), and solubility (at 100,000 mg/L) (c) of a pure component as a function of depth.	7
Figure 2. Cross section of generic model displaying homogeneous field with baffles (a) and heterogeneous permeability field (b).	7
Figure 3. Mixture density (a) and density to viscosity relative to neat CO ₂ (b) as a function of depth; hydrostatic conditions and geothermal gradient of 18°C/km and 33°C/km.	7
Figure 4. Illustration of how maximum extent and time to reach the top are extracted from run results.	8
Figure 5. Plume-extent-increase for binary CO ₂ systems compared with pure CO ₂ plume extent 100 years after start of injection for N ₂ , Ar, O ₂ , CH ₄ , CO, and H ₂ . Horizontal axis represents impurity molar-fraction range (0–25%).	9
Figure 6. Illustration of sample mineralogical composition	12
Figure 7. Unreacted and reacted Offshore Miocene samples	15
Figure 8. Unreacted and reacted Cranfield samples	16
Figure 9. Unreacted and reacted Cardium samples	17
Figure 10. Impact of dissolution at gas composition at plume front	21
Figure 11. Mixture density relative to neat CO ₂ as a function of depth.	22
Figure 12. Mixture density-viscosity ratio relative to that of neat CO ₂	23

List of Tables

Table 1. Molar composition of base cases	6
Table 2. Characteristics of shallow and deep generic models.	6
Table 3. Comparison of Stream A, stream C, and neat CO ₂ (base case) plume extent in various conditions of heterogeneity (shallow case).....	6
Table 3. Summary of sample mineralogical composition	11
Table 4. Summary of geochemical runs	13
Table 5. Partial list of autoclave runs.....	14
Table 6. Trace element impact.....	19

Acknowledgments

The authors would like to thank the CO₂ Capture Project Phase 3 for funding this project and, in particular, the project manager, Scott Imbus. We are also grateful to the Computer Modeling Group (CMG), Calgary, Canada, for giving us ~free access to their GEM software and ECRB for providing the Cardium samples for the autoclave experiments. We are also grateful to the DOE-sponsored SECARB project for providing the Cranfield samples, and to the DOE- and State of Texas-sponsored Mega-Transect Carbon Repository project for providing the Miocene samples.

Acronyms

ACPP	Alberta CO ₂ Purity Project
BEG	Bureau of Economic Geology
CCP3	CO ₂ Capture Project Phase III
IFT	Interfacial tension
PVT	Pressure, temperature, volume
USDW	Underground sources of drinking water

I. Introduction

This report documents findings of a project funded by Phase III of the CO₂ Capture Project (<http://www.co2captureproject.org/>) (CCP3). CCP3 is a partnership of six major energy companies interested in advancing the technologies that will support the deployment of industrial-scale CO₂ capture and storage. The work addresses some of the issues related to non-pure CO₂ streams. Geologic sequestration of carbon dioxide (CO₂) is poised to become an important technology for addressing high CO₂ atmospheric concentrations and global warming. The impurities of interest consist of N₂, O₂, H₂, CO, Ar, SO_x to which CH₄, common in the subsurface, can added, and are present (incidental to the capture process) at a range of concentrations in the injected CO₂ stream. However, little work has been done to explain the impact of impurities on subsurface behavior of the CO₂-dominated injection stream. The report summarizes findings from two earlier reports dedicated to predicting some aspects of the impact of impurities on large scale CO₂ plume behavior (Nicot and Solano, 2012) and on smaller scale geochemical processes that may impact injectivity (Nicot et al., 2013). It also explores the interaction between flow and geochemistry (Task 5 below). However, the work does not address legal and regulatory issues such as the permissible level of impurities before which an injection scheme would become a waste disposal operation rather than a CO₂ injection operation.

Opportunities to reduce capture costs provided the incentive to investigate the impact of impurities on non-condensable impurities on reservoir system dynamics and geochemical changes in the injection formation and their consequences on flow and ultimate capacity. Leaving some of the impurities in the injection stream could save both capital and operational costs possibly without significant economic or HES (health, environment, safety) assurance consequences to the storage part of the project. For example, pipelines and compressors could be re-engineered to handle impurities. On the other hand, power generation and industrial processes that have CO₂ as a byproduct seldom produce a pure CO₂ stream. When the CO₂ fraction is low (as is the case of flue gas from conventional power plants), an amine-based capture system that will increase the CO₂ fraction (to >99%) and possibly eliminate most of the impurities is needed and highly desirable. However, when the CO₂ fraction in the waste stream is already high (e.g., oxyfiring or gasification), only some level of gas processing might be required, depending on the subsurface characteristics of the strata that are to receive the stream and on other local operational factors (i.e., if compression, transportation not unduly impacted or can be cost-effectively re-engineered). This paper proposes to explore the impacts of impurities on CO₂ behavior in the subsurface during geological carbon storage. Impacts can be classified into two types: (1) direct impact on flow behavior and (2) geochemical impact and indirect impacts on flow. Simulations of CO₂ injection floods with selected impurities levels were conducted on generic models broadly representative of major onshore / near-shore clastic systems in North America and Europe (low to moderate permeability). This work does not include potential geochemical modification of the impure injection stream on porosity and permeability or dry-out effects in the near wellbore area.

The technical tasks consisted of:

1. Accessing PVT data through a literature search and conducting new PVT experimental work to fill in gaps.

2. Conducting a parametric study on impact of impurities on plume dynamics and rate and extent of trapping mechanisms in saline aquifers. This task is mostly a desktop numerical study performed with synthetic simplified cases and generalized models of actual reservoirs.
3. Conducting rock-fluid interaction studies, including modeling and autoclave experiments.
4. Conducting reactive transport numerical modeling
5. Integrating the results to qualitatively assess the impact of gas impurities on (1) plume shape and evolution, (2) CO₂ permanence (trapping), (3) CO₂ storage capacity, (4) well injectivity, (5) storage reservoir integrity, and (6) trace elements released/absorbed during dissolution / precipitation caused by addition of impurities.

Overall, the objectives of the project are (1) to understand plume dynamics as it impacts Area of Review and permanence / containment / leakage (including impacts on trapping mechanisms); (2) to assess impact on capacity; and (3) to assess impact on injectivity.

The contract between CCP3 and the Bureau of Economic Geology at the University of Texas at Austin (BEG) was executed in December 2009 with an end date of March 31, 2011. It was subsequently extended to September 30, 2012 with additional tasks, in particular related to the Alberta CO₂ Purity Project (ACPP). Ms. Silvia Solano performed and processed most of the flow simulations whereas Dr. Johns completed experimental work to access PVT information on the different gas mixtures. Drs. Lu, Mickler, Yang, and Romanak supported the geochemical work.

The focus of the study is on the behavior of the flue-gas streams of gas oxy-fired power plants (combustion in ~pure O₂). Impurities in the flue streams include N₂, Ar, O₂, CO, and, potentially, H₂, SO_x, NO_x, and other acid species. The analysis of impact of impurities on flow behavior included four gases: CO₂, N₂, Ar, and O₂ whereas the geochemical analysis focused on the only two reactive gases CO₂ and O₂. CO₂ capture experts have not converged yet to a small set of applicable technologies but a range of compositions can be inferred from the literature (see Nicot and Solano, 2012). Discussions with industry experts, however, suggested that maximum volume fractions are 15% for N₂ (that is, ~10% molar in a binary mixture), 5% for Ar and O₂, 2% for CO, and 0.15% for SO_x (see Table 2 for corresponding densities). Once the impure CO₂ stream is injected into the subsurface, CH₄ and H₂S gases, which are commonly present in brines in a dissolved state in many basins, can form a significant percentage of the mixture as they partition from the brine into the supercritical phase. This phenomenon could occur to some degree even if the injected stream is composed of only pure CO₂. At this point, a comparison between density and viscosity of the main mixture components could be helpful because they vary with depth. In the subsurface, temperature and pressure are positively correlated, and an exploration of the entire P, T space (Fig. 1) is not needed. Pressure can be assumed to be hydrostatic in most settings, and the temperature gradient varies within a relatively small range (15–35°C/km). Density values of all impurities are significantly less than that of CO₂ by at least a factor of 2, with CO₂>>Ar>O₂>N₂>CH₄. Viscosity values follow the same pattern below the depth at which CO₂ mixtures are supercritical.

Whereas impurities can have a plume-wide impact because of changes in flow properties, geochemical reactions are more likely to impact the near-field, where reactive species can be consumed. Reactive gases potentially include O₂, CO, SO_x, NO_x, and minor acid species such as HCl, HCN, and bases such as NH₃. Rock-mineral components can dissolve, possibly increasing porosity, permeability, and injectivity, but also compromising the stability of the well. Conversely, authigenic minerals can precipitate and impede flow by decreasing permeability.

II. Flow Dynamics Findings

II-1. Summary of Flow Dynamics Findings

The goal of this part of the study was to understand the impact of impurities (N_2 , O_2 , and Ar, to which was added CH_4 , ubiquitous in the subsurface in hydrocarbon provinces, often prime candidates for geological storage) on CO_2 plume dynamics, injectivity, and capacity. The study considered up to 15% volume for N_2 , 5% volume for O_2 , and 5% volume for Ar. Other gases such as CO, H_2 , and SOx, which could have non-negligible mole fractions, are not considered in this part of the study. The problem was approached through an extended desktop study using the numerical modeling tool (multiphase flow code CMG-GEM). In order to work with accurate PVT data (Peng-Robinson EOS), laboratory experiments were performed early in the study to access viscosity and density of the mixtures. CMG-GEM relies on many empirical mixing rules for density and viscosity calculations that need to be calibrated and tuned (Figure 1). In parallel, a comprehensive literature survey was undertaken to collect information on solubility of those various mixture components into the aqueous phase under various subsurface pressure, temperature, and salinity conditions. The differential partitioning of gas components in the aqueous phase impacts the gas phase composition. The work presented in this section does not include geochemical impact of impurities (reactivity of gas components with other components and with minerals). Overall, geochemical processes could affect near-field properties such as injectivity and well integrity whereas larger-scale regional impacts on plume dynamics are likely only an issue with significant mole fractions of non-condensable gases (including O_2). An important observation integral to understanding plume dynamics associated with impurities is that viscosity and density of mixtures are lower than that of neat CO_2 at the same temperature and pressure. Equally important to note, viscosity and density contrasts between mixtures and neat CO_2 decreases with depth.

The numerical models used grow in complexity from simple box-like generic models, to which heterogeneity is added in a second step, to more realistic models constructed from actual U.S. Gulf Coast locations but representative of many sites around the world. The objective was to reproduce end-members of aquifer architecture such as (1) clean homogeneous, medium permeability sand; (2) homogeneous sand/clay, and (3) heterogeneous sand with discontinuous shale partings and continuous baffles. Progressively more complex gas systems, binary, ternary, and beyond, were investigated. The results, normalized by results of the corresponding neat CO_2 case, draw on two metrics, time to hit the top and maximum longitudinal extent. These are contrasted for two depths “shallow” (~5,000 ft, ~60°C, 2500 psi, 100,000 mg/L) and “deep” (~10,000 ft, 125°C, 4500 psi, 180,000 mg/L). Because O_2 , N_2 , and Ar have similar properties and behavior, they impact the CO_2 -dominated mixtures in a similar way, particularly at the concentration level of a couple percent molar and they can be merged in one unique component with properties of N_2 . However, the approximation deviates too much from the “truth” beyond a few percentage points.

Impurities impact density and viscosity of the CO_2 -rich mixture. A lower density impacts CO_2 capacity not only because of the smaller fraction injected and space needed for storing impurities but also because of the generally lower density of the impurities at the same conditions. An approximate proxy for capacity change owing to impurities is given by the density ratio. The loss in capacity can be as high as >50% at very shallow depths (~3000 ft, CO_2 and 15% molar N_2) but

the difference quickly decreases with depth. Similarly, mass injectivity, which can be represented by the proxy metric of density over viscosity ratio, also shows a decreased value at very shallow depths that quickly recovers with increasing depth.

In terms of plume shape and extent, the impact of impurities is again more marked at shallow depth where the contrast in density and viscosity with neat CO₂ is the largest. It decreases with depth. For example, about 4% mole fraction in a binary system suffices to increase plume length in “shallow” low-dip sloping layers by 25% whereas 9 to 15%, depending on the component, would be the case in a “deep” system. In all cases, plume extent is greater with impurities however residual trapping occurs faster. This relationship holds for most systems regardless of heterogeneity and complexity. The contrast is most extreme in very simple systems whereas heterogeneity (assuming adequate operational choices) seems to dampen impacts of impurities. This presumably occurs because heterogeneity creates multiple tongues that attenuate the impact of impurities. It also suggests a trade-off between plume extent (area of review with risk of CO₂ leakage) and decreased risk owing to faster trapping. A larger plume translates into a larger area to inspect for leakage pathways such as faults and abandoned wells but a faster trapping translates into a shorter period of time to monitor the site.

II-2. Illustration of Key Flow Dynamics Findings

The general approach consisted of a parametric study and sensitivity analyses of a generic case and of three previously studied sites (two on the U.S. Gulf Coast and one in Alberta, Canada), modified slightly to meet our objectives. Gas composition and range were estimated from various sources (Table 1); see Nicot and Solano (2012). Because of the lack of accurate data on viscosity and density, we performed 10 experiments (through an external vendor based in Houston, Texas) to tune EOS parameters for various CO₂ mixtures (incorporating CO₂, N₂, O₂, and Ar) at various temperatures (60, 80, and 100°C) and pressures (13.8, 27.6, and 41.4 MPa). We also developed binary interaction coefficients between components under a range of pressure (10–50 MPa), temperature (30–120°C), and salinity (0–200,000 mg/L) conditions through a comprehensive literature audit so as to model dissolution of the mixtures into the brine. We initially used a simple dual generic model: a shallow model reproducing conditions present at the Frio site (southeastern Texas) and a deep model reproducing conditions prevailing at Cranfield (western Mississippi). Both sites are in the U.S. Gulf Coast region, but for analysis they were stripped of specific properties, retaining only environmental conditions: pressure, temperature, and salinity (Table 2). In order to focus on the processes of interest and not on specificities associated with an actual site, we developed a generic sloping aquifer and compared results of runs carried out using various CO₂ mixtures. Runs were performed using the CMG-GEM and CMG-WINPROP software packages. GEM is a compositional multiphase flow code that can accommodate multiple gas components and their interaction with a liquid phase. WINPROP is an allied module useful in determining and tuning equations of state.

The only trapping mechanisms simulated in the model were dissolution and residual-phase mechanisms. Mineral-phase trapping on a meaningful scale is generally understood to require at least hundreds or thousands of years. Structural trapping—that is, trapping of CO₂ as would occur in oil and gas accumulations—was not included in the design of the generic model because structural trapping would be of negligible utility in explaining the interplay of all processes and is site specific. The model was large enough (11 km) for the CO₂ mixtures to be fully trapped as residual saturation before reaching the updip boundary, assuming an injection rate equivalent to

0.5 million tons of pure CO₂ for 30 years. Injection occurred at the downdip section of the lower third of the 300-m-thick reservoir (Figure 2). Results are to be understood relative to one another, in particular relative to the base cases, because of numerical and gridding issues. For example, in homogeneous models, plume extent is a function partly of cell size but mostly of cell height (Thibeau and Dutin, 2011; they investigated the largest cell thickness that would model CO₂ dissolution correctly in their model and concluded that it is <0.1 m). Scaling the plume extent from various runs to the pure CO₂ base case minimizes this effect.

The metrics used to measure impact on storage consisted of (1) time for the plume to reach the top and, more important, (2) extent of the plume at a given time or when all of the injected CO₂ mixture had been immobilized, and (3) time until all CO₂ mixture was immobilized (Figure 4). After treating the homogeneous case, we developed reservoir models encompassing a range of heterogeneity: (1) we handled heterogeneity in a simplistic way by adding four baffles with no porosity, parallel to the formation top and bottom, just upstream of the injection well and short of a few cells, all the way up to the updip boundary and across the whole width of the model (Figure 2a); (2) we obtained multiple heterogeneous fields through permeability generators (Figure 2b); and (3) we used models from actual sites.

First, we estimated static capacity, which is especially relevant to the case of structural traps because it relates to the volume occupied by the mixture in the subsurface. Comparison of densities as a function of depth allows for a first-order comparison of capacities. Second, we examined dynamic capacity. Results are consistent with that of a previous IEAGHG study (IEAGHG, 2011; Wang et al., 2011). They addressed topics very similar to those discussed in this document. They focused on the capacity issues and reported that non-condensables such as N₂, O₂, and Ar impact capacity and that the impact is maximal at a certain pressure under a given temperature. Impurities impact static capacity by causing variations in density and viscosity of the CO₂-rich mixture. A lower density impacts CO₂ capacity not only because of the smaller fraction of CO₂ that can be injected and space taken up by impurities, but also because of the generally lower density of the impurities under the same conditions. An approximate proxy for capacity change owing to impurities is provided by the density ratio. The loss of capacity can be >50% at shallow depths (~3000 ft, CO₂ and 15% molar N₂) (Figure 3), but the difference quickly decreases with depth. Similarly, mass injectivity, which measures how much CO₂ can be injected (and which can be represented by the proxy metric of the density:viscosity ratio), also exhibits a value that decreases at shallow depths but recovers with increasing depth.

Dynamic reservoir simulations revealed that, following the pattern of static capacity and for the same reasons, impurities impact CO₂ plume shape (rate of vertical ascent and lateral extent) more markedly at shallow depths where the contrast in density and viscosity with pure CO₂ is at its largest. For example, a 4% mole fraction impurity in a binary system is sufficient to increase plume length in ‘shallow’ low-dip sloping layers by 25%, whereas a mole fraction of 9 to 15%, depending on the component, is needed to create the same impact in a ‘deep’ system (Figure 5). Note that pure-CO₂ plume extent is larger at depth than in the shallow case, but that the difference between streams of pure CO₂ and CO₂ with impurities is smaller in the deep model.

In all cases, plume extent is greater when impurities are present, although residual trapping occurs more rapidly. This is generally the case regardless of reservoir heterogeneity and complexity, although heterogeneity tends to moderate the impact of impurities on plume extent because of the multiplicity of smaller plumes (Table 3, see Nicot and Solano, 2012 for details). Note that heterogeneity tends to increase plume extent because although CO₂ favors higher-

permeability streaks, the contrast between pure CO₂ and CO₂ with impurities is smaller. Overall, a trade-off occurs between larger plume lateral extent owing to the presence of impurities and decreased risk owing to faster trapping (pressure management).

Table 1. Molar composition of base cases

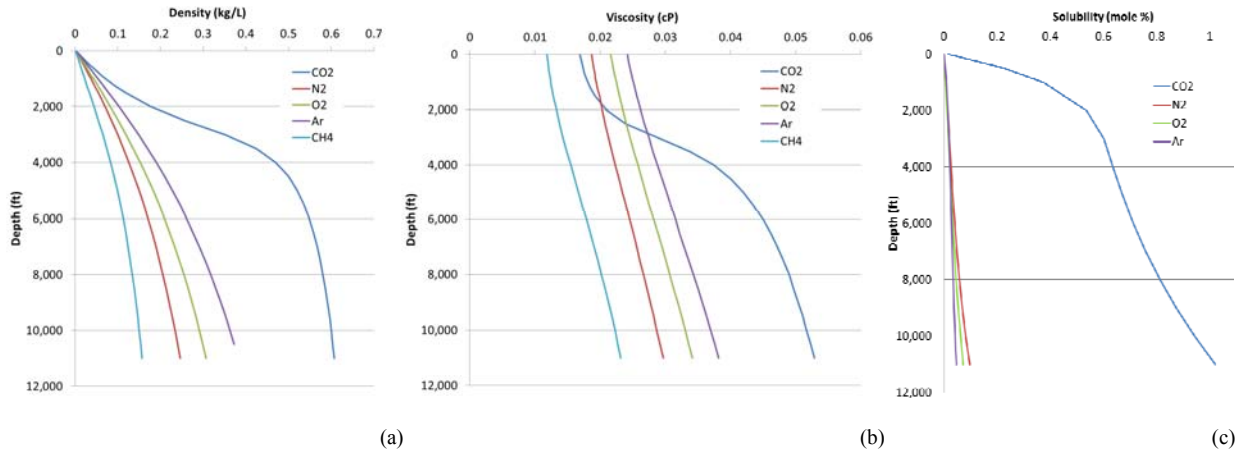
Component (mol %)	Neat CO ₂	Stream A	Stream C	Single component density at 1 atm and 21°C (kg/m ³)
CO ₂	100	96	92	1.834
N ₂	—	0.2	1	1.161
O ₂	—	2.1	6.5	1.327
Ar	—	1.7	0.5	1.654
CO	—	—	—	1.162

Table 2. Characteristics of shallow and deep generic models.

Reservoir Property	Shallow Reservoir Case	Deep Reservoir Case
Model dimensions	11,000 × 4660 × 300 m ³	same
Number of cells x × y × z	120 × 51 × 20	same
Cell dimensions	90 × 90 × 15 m ³	same
Dip in x direction	2°	same
Permeability /kv/kh / porosity	300 md / 0.01 / 0.25	same
Depth at top downdip	1675 m	3040 m
Initial pressure (equilibrium at time 0)	V.E. ~17.6 MPa at top downdip	V.E. ~32.4 MPa at top downdip
Temperature	135°F	257°F
Injection rate and period	8.5 m ³ /s for 30 years	same
Maximum res. saturation	0.30	same
Boundary	No flow except updip (hydrostatic)	
Formation water TDS	~100,000 mg/L	~170,000 mg/L
Simulation period	100 yr	same

Table 3. Comparison of Stream A, stream C, and neat CO₂ (base case) plume extent in various conditions of heterogeneity (shallow case)

(ft)	Uniform	w/ Baffles	Real#7	Real#8	Real#9	Real#10	Real#13
Neat CO ₂	9,300	8,400	10,500	6,900	5,100	5,100	7,200
Stream A	11,400	9,300	15,300	7,200	5,400	5,100	7,800
Stream C	14,400	10,800	19,800	7,500	5,400	6,900	7,800
A / neat ratio	1.23	1.11	1.46	1.04	1.06	1.00	1.08
C / neat ratio	1.55	1.29	1.89	1.09	1.06	1.35	1.08



Note: SO₂ would have an opposite impact; hydrostatic pressure and geothermal gradient of 22°C/km

Figure 1. Density (a), viscosity (b), and solubility (at 100,000 mg/L) (c) of a pure component as a function of depth.

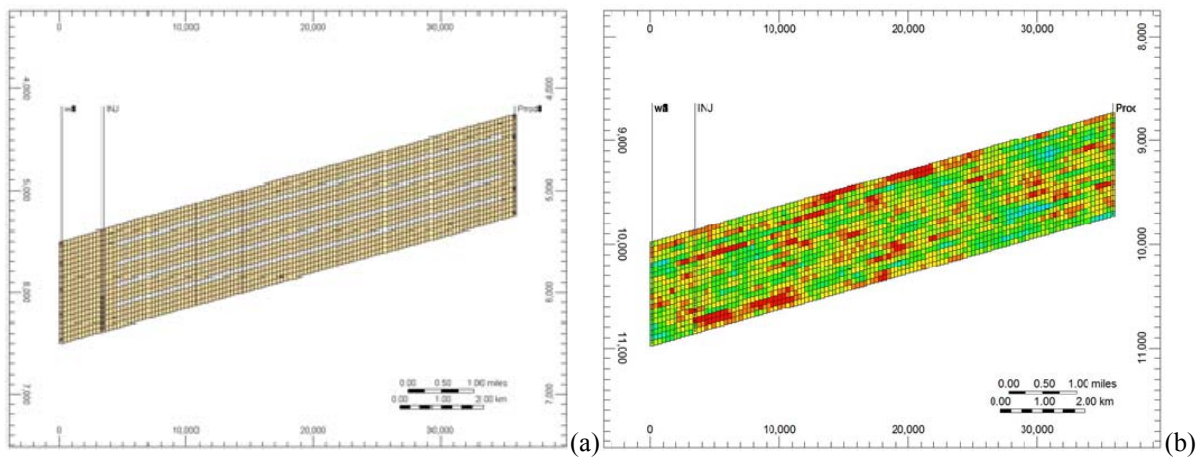


Figure 2. Cross section of generic model displaying homogeneous field with baffles (a) and heterogeneous permeability field (b).

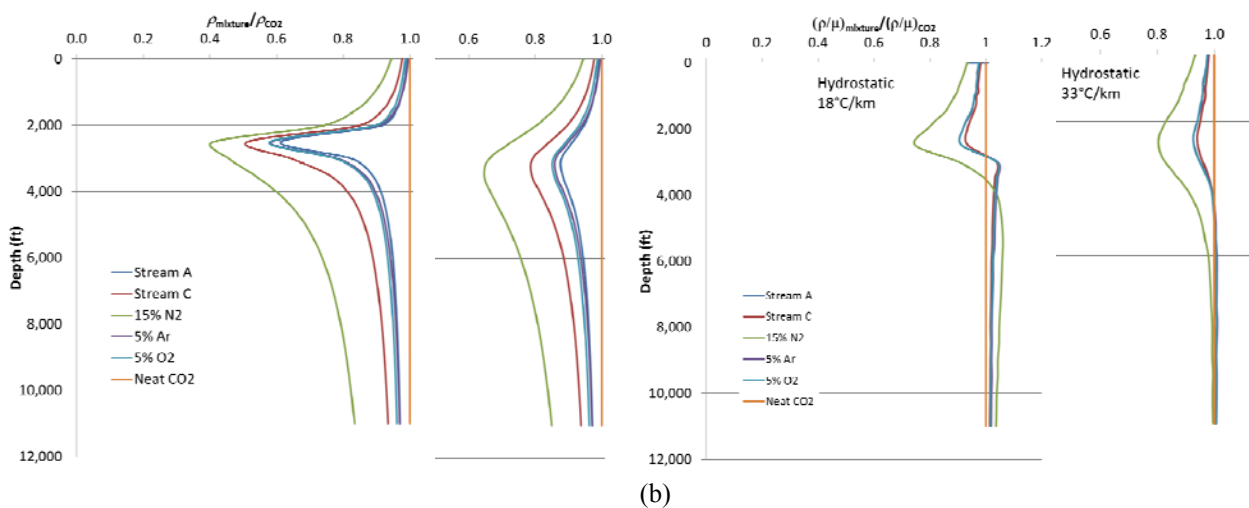


Figure 3. Mixture density (a) and density to viscosity relative to neat CO₂ (b) as a function of depth; hydrostatic conditions and geothermal gradient of 18°C/km and 33°C/km.

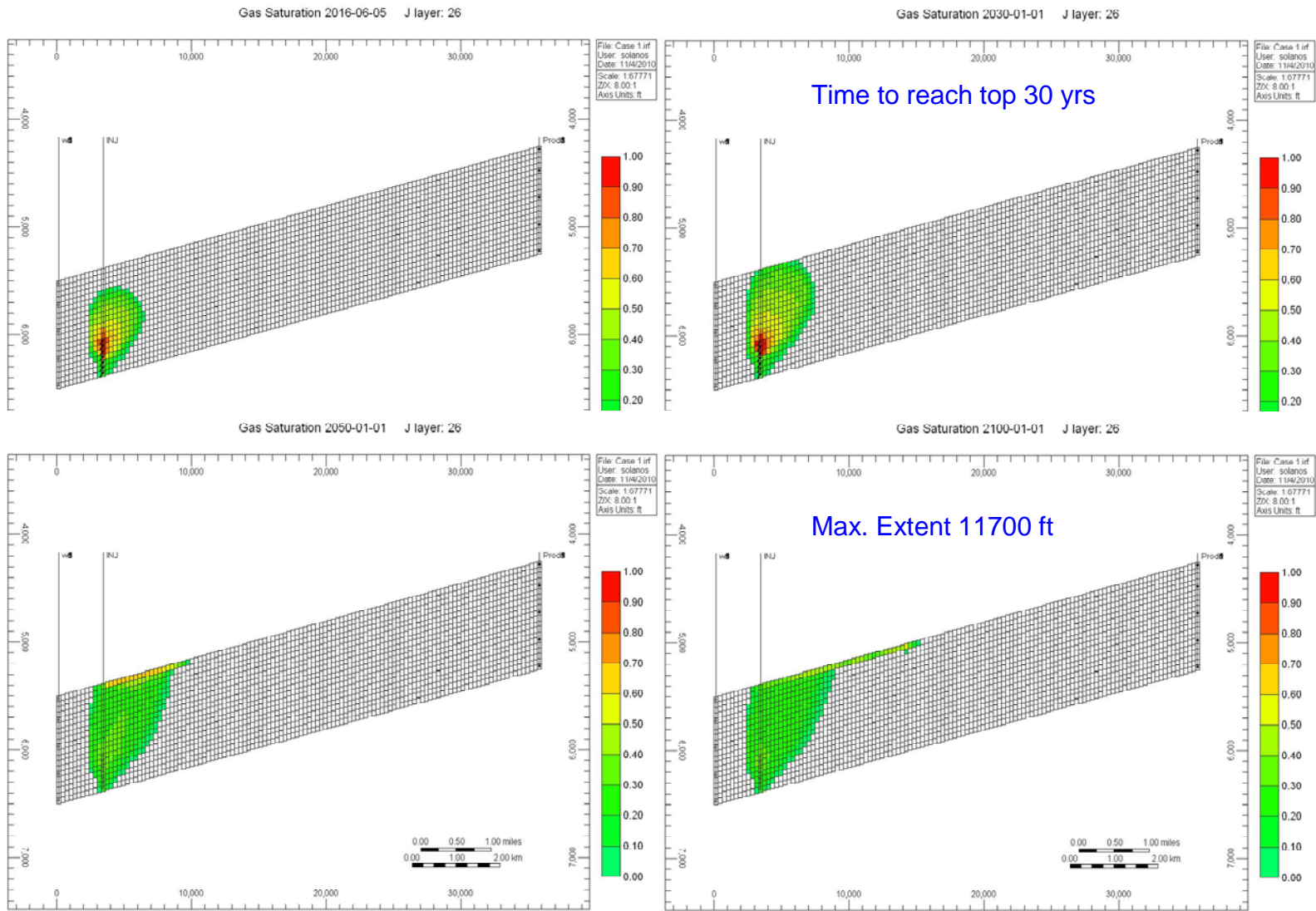
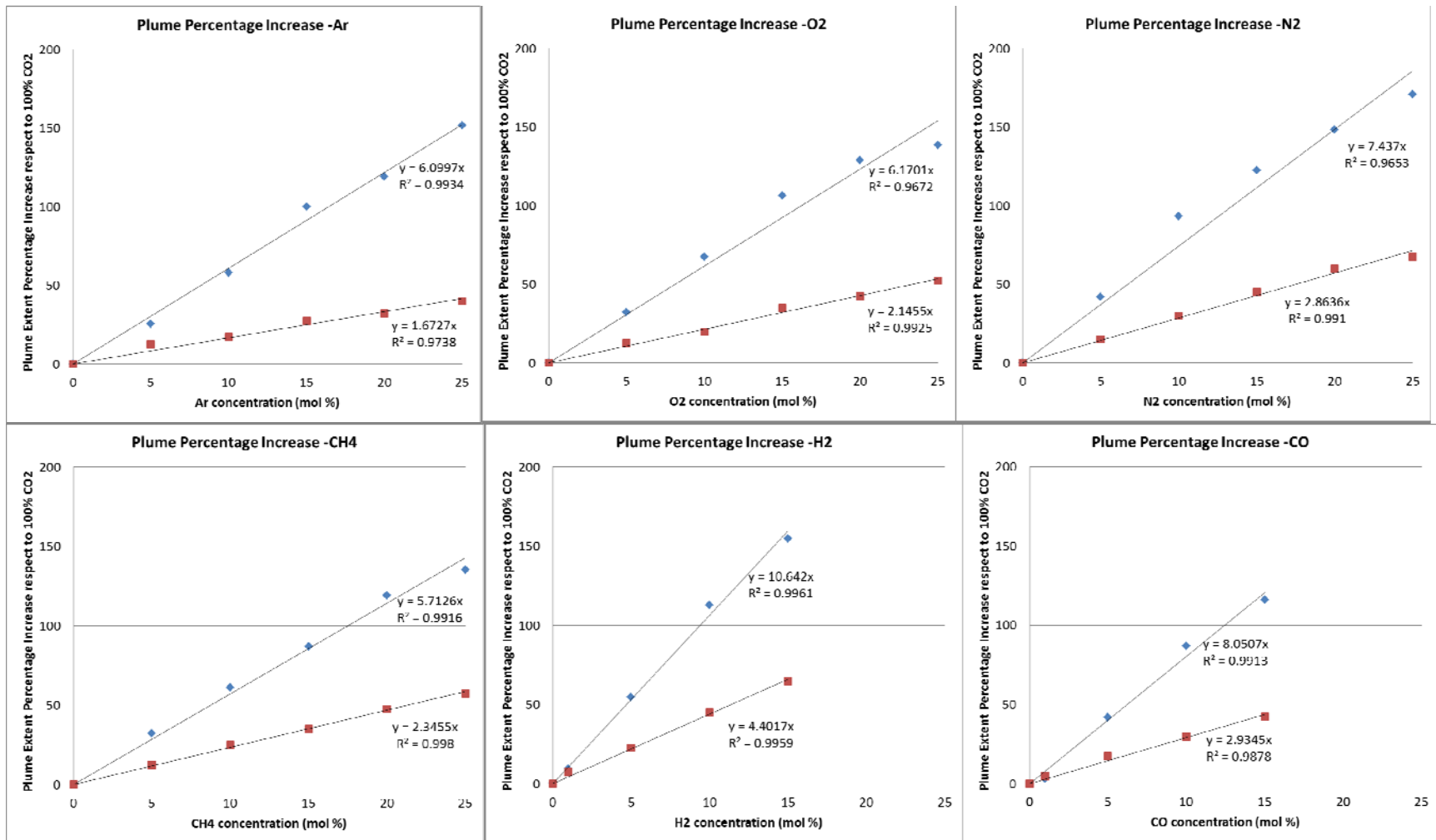


Figure 4. Illustration of how maximum extent and time to reach the top are extracted from run results.



Note: Vertical axis displays additional extent; that is, 100% means a doubling of plume length. Linear fitting by forcing straight line through origin.

Figure 5. Plume-extent-increase for binary CO₂ systems compared with pure CO₂ plume extent 100 years after start of injection for N₂, Ar, O₂, CH₄, CO, and H₂. Horizontal axis represents impurity molar-fraction range (0–25%).

III. Geochemistry Findings

III-1. Summary of Geochemistry Findings

The geochemical issue is approached through laboratory autoclave experiments coupled with geochemical numerical modeling. The autoclave consists of a 250-ml reactor able to sustain temperatures as high as 150°C and pressures as high as 400 bars, that is, conditions seen in reservoirs up to a depth of 12,000 ft. A computer automatically regulates pressure and temperature and the system also allows for water sampling during the experiments. Typically 10 to 15 samples of the solution were taken during the 5-to-10 day course of each of the experiments. Rock samples were exposed to a supercritical mixture of CO₂ and O₂ (in general 3.5% molar) or to pure supercritical CO₂ that filled about half of the reactor cell. The other half consisted in a single core fragment or a few large fragments (~8g total) submerged into ~140 ml of synthetic brine (~1.88 mol NaCl corresponding to a TDS of 100,000-110,000 mg/L). The study analyzed three clastic rock samples: (1) a “dirty sandstone” of Miocene age from a deep well in the shallow offshore off the Texas coast; (2) a relatively clean sandstone from the Cardium Formation of Cretaceous age from Alberta; (3) a chlorite-rich sandstone from the Tuscaloosa Formation in Mississippi originating from the Cranfield site that BEG has been thoroughly studying for several years. Composition of the samples is presented in Table 4 and Figure 6.

Table 4. Summary of sample mineralogical composition

	Offshore Miocene, TX Well OCS-G-3733 Depth 9205 ft	Cardium Sands, AB Well unknown Depth unknown	Cranfield, MS Tuscaloosa Formation Well CFU31F-3 Depth 10,476.6 ft
Quartz	43.5%	75.5%	66.9%
Calcite	11.8%		
Siderite		1%	
Microcline	15.2%	4.2%	
Albite	18.4%	2.5%	1.8%
Chlorite			20.2%
Kaolinite	6.2%	10.4%	7.3%
Illite	5.0%	6.5%	2.0%
Pyrite	Trace++	Trace+++	Trace (barely)
Anatase			1.8%
Total	100.1%	100.1%	100%

In addition to quartz, the Miocene sample is dominated by calcite (11.8%) and feldspars (31.6%), the Cardium sample is dominated by clays (16.9%) with some feldspar (6.7%) and siderite (~1%), and the Cranfield sample is dominated by chlorite (20.2%) with some clays (9.3%). Both the Miocene and Cardium samples show evidence of not uncommon pyrite. The “dirty sandstone” Miocene sample allows for investigating carbonate behavior with and without O₂ whereas the relatively clean and non-reactive Cardium sample is a good candidate to investigate feldspar behavior without the overprint of carbonates. The Cranfield sample with abundant clay minerals dominated by chlorite is even less reactive vis-à-vis CO₂. Minerals sensitive to the presence of O₂ are pyrite (present in the Miocene and Cardium samples), siderite (present in the Cardium sample), and chlorite (abundant in the Cranfield sample). They all contain ferrous iron-bearing minerals.

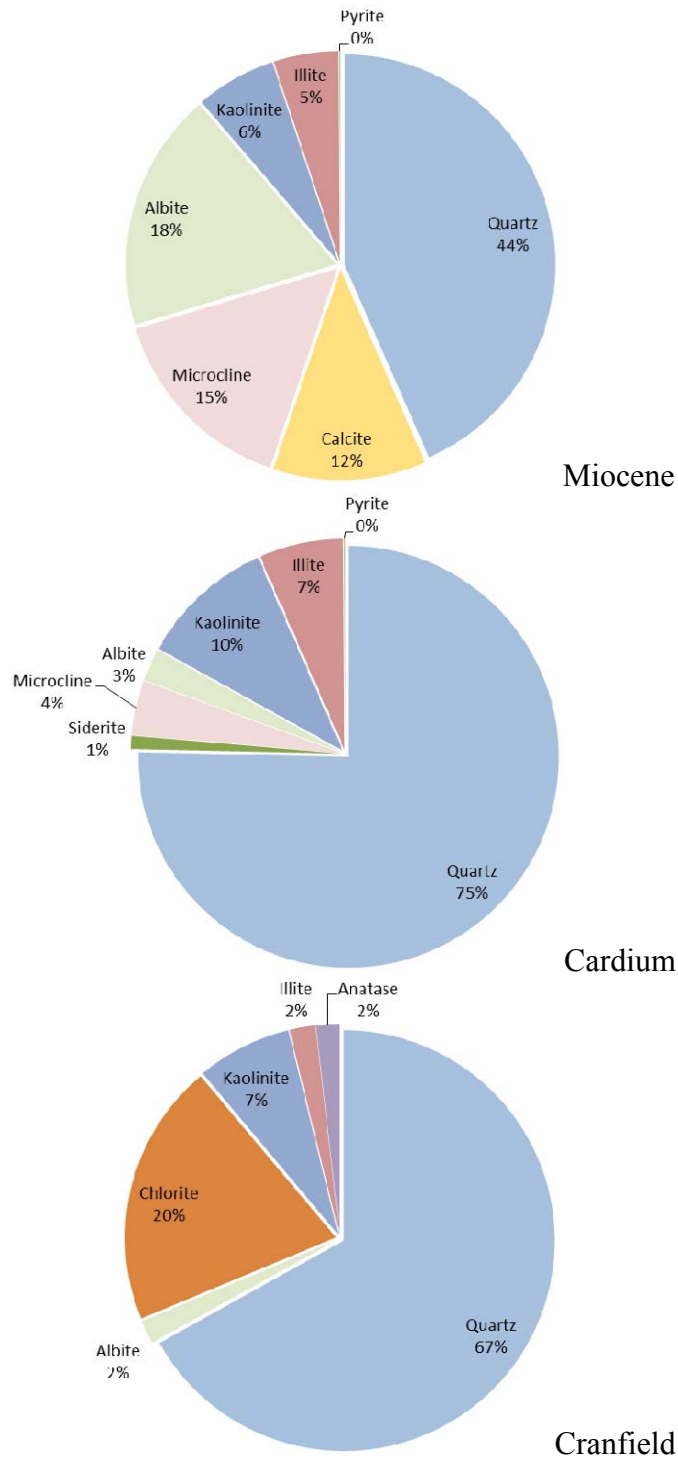


Figure 6. Illustration of sample mineralogical composition

We performed 19 autoclave experiments varying some parameters but only 10 are thoroughly described. They are displayed in the matrix of Table 5. Core segments with pre- and post-reaction rocks were submitted to petrographic analyses (X-ray diffraction –XRD, scanning electron microscope –SEM, and energy dispersive X-ray spectroscopy –EDS) and chemical analyses (TDS, anions, cations, trace elements).

Table 5. Summary of geochemical runs

		70°C	100°C	130°C
Offshore Miocene	CO ₂	√ D	√ L (B)	√ H
	CO ₂ + O ₂	√ R	√ S	
Cardium Sands	CO ₂	√ K	√ J	
	CO ₂ + O ₂	√ N		
Cranfield	CO ₂	√ P		
	CO ₂ + O ₂	√ O		

Note: numbers correspond to individual runs

The offshore Miocene samples showed dissolution of carbonate (Ca and Mg increase) as well as of feldspars (Ca and K increase, Na concentrations are irrelevant because experiments are done with a NaCl brine). Feldspar dissolution is more intense when O₂ is present. Kaolinite is presumed to form in both cases. The Cardium samples displayed deep attack of carbonates and of some feldspars with kaolinite formation and perhaps very minor authigenic illite. Pyrite and siderite are degraded when O₂ is added and FeOx species precipitate. The Cranfield samples have limited reactivity when exposed to pure CO₂ as they contain little carbonates. When O₂ is added, some chlorite is degraded and FeOx deposits can be observed as well as formation of some authigenic clays. Those qualitative observations were confirmed by geochemical modeling which was able to reproduce them.

In terms of release rates, results confirmed well-known results and delivered new observations. In pure-CO₂ cases carbonates were observed to dissolve quickly with a sharp increase in Ca, Mg, and other elements typically present in calcite. Calcite solubility was also observed to decrease with increasing temperature (i.e., reverse solubility). As expected, feldspars showed an increase in solubility with increasing temperature whereas clays, including chlorite, remained unreacted. Adding O₂, however, brought in interesting observations, pyrite framboids were clearly degraded, and thus added H⁺ ions to the system with consequent increased carbonate dissolution. The siderite (Cardium sample) is another source of ferrous iron. Both pyrite and siderite attack led to deposition of FeOx on mineral surfaces. Chlorite could also be an important source of ferrous iron but it is mostly stable unless pH drops very low. Such a case could happen if pyrite is present at a few percent level and lack of pH-buffering capacity through carbonates. Some chlorite alteration was seen in the Cranfield sample. Early in the study it was believed that O₂ had a catalytic effect on dissolution of other minerals. It turns out that, corrected for CO₂ fugacity, the speculated effect of O₂ disappears when considering carbonate dissolution. Feldspar dissolution is enhanced in the presence of O₂ but in an indirect way, through pyrite oxidation and drop in pH. Overall the additional impact of a few percent O₂ when comparing samples reacted with pure CO₂ and with a CO₂+ O₂ mixture is limited. The observation is also true for trace elements released to the brine following mineral dissolution; concentration in some cases increased several-fold, but never at a level high enough to generate a drinking water hazard when diluted with fresh water (relevant if saline waters contacted by CO₂ with impurities were to invade and aquifer). Aqueous concentrations of several elements (V, Mo, As) drop when O₂ is added because they form oxyanions that sorb to precipitating FeOx and clays. We also looked at other reactive species contained in the gas stream (CO, H₂, SOx, and other trace gases) from a modeling standpoint and in particular the concentrations at which they would have an impact on the pH of the solution. They would start having an impact on pH (and therefore on carbonates

and feldspar dissolution) at concentrations ranging from 100 to 1000 ppm depending on depth and reservoir conditions.

Although the following results need to be confirmed by column (coreflood or flow) experiments, the reactive transport modeling suggests that porosity changes due to mineral reactions in siliciclastic material is minor and that mineral precipitation is unlikely to impact fluid flow. Overall, it does not seem that a few percent O₂ in the CO₂ stream has much impact beyond the impact of neat CO₂.

III-2. Illustration of Key Geochemical Findings

A summary of key autoclave runs is presented in Table 6. To understand kinetics of interaction among brine-CO₂-O₂-rocks and release rates to the brine, we need to look at major ions (Ca, K, Mg; Na results are obscured by the use of a NaCl brine) but also at Al and Si of water samples. Ca and Mg concentration trends reflect carbonate dissolution whereas Al and Si concentrations are important to quantify kinetics of silicate mineral reactions. K and Na cannot provide enough information to quantify the kinetics of silicate mineral dissolutions. Alkalinity and sulfate concentrations indicate bicarbonate levels and gypsum / anhydrite and possibly pyrite dissolution, respectively. Fe is also a relevant indicator of the system behavior.

Table 6. Partial list of autoclave runs.

Experiment	Temperature (°C)	Pressure (bars)	Fluid	Sample Origin	Sample weight (g)	Brine volume (ml)	Comments
D	70	200	1.88 mol/kg NaCl sol.	Miocene	6.65	155	0% O ₂
H	130	200	1.88 mol/kg NaCl sol.	Miocene	6.43	140	0% O ₂
J	100	200	1.88 mol/kg NaCl sol.	Cardium	8.45	140	0% O ₂
K	70	200	1.88 mol/kg NaCl sol.	Cardium	8.03	140	0% O ₂
L	100	200	1.88 mol/kg NaCl sol.	Miocene	7.26	140	0% O ₂ , re-run of series B
N	70	200	1.88 mol/kg NaCl sol.	Cardium	10.39	110	3.5% O ₂
O	70	200	1.88 mol/kg NaCl sol.	Cranfield	8.11	110	3.5% O ₂
P	70	200	1.88 mol/kg NaCl sol.	Cranfield	8.44	110	0% O ₂
R	70	200	1.88 mol/kg NaCl sol.	Miocene	8.40	110	7% O ₂ (200 psi)
S	100	200	1.88 mol/kg NaCl sol.	Miocene	8.89	110	3.5% O ₂ (100 psi)

Trace elements have in general two origins: they are (1) contained in minute amounts in major minerals (such as Sr in calcite or Cs in K-feldspar) in which case their concentrations will trend similarly to that of the major elements or (2) mobilized from sorbing material such as FeOx grain

coatings or clay mineral edges (kaolinite and illite). Addition or destruction of sorbing material can complicate the interpretation of trace element behavior. Ion exchange is unlikely to play a major role because the samples as a whole have little exchangeable capacity (a few percent illite that could be mixed-layered) or no capacity in the more common chlorite and kaolinite.

The Miocene samples display a more thorough degradation of carbonates and particularly feldspars relative to pure CO₂ case when O₂ is added; the likely impact of minor pyrite oxidation and related pH drop.

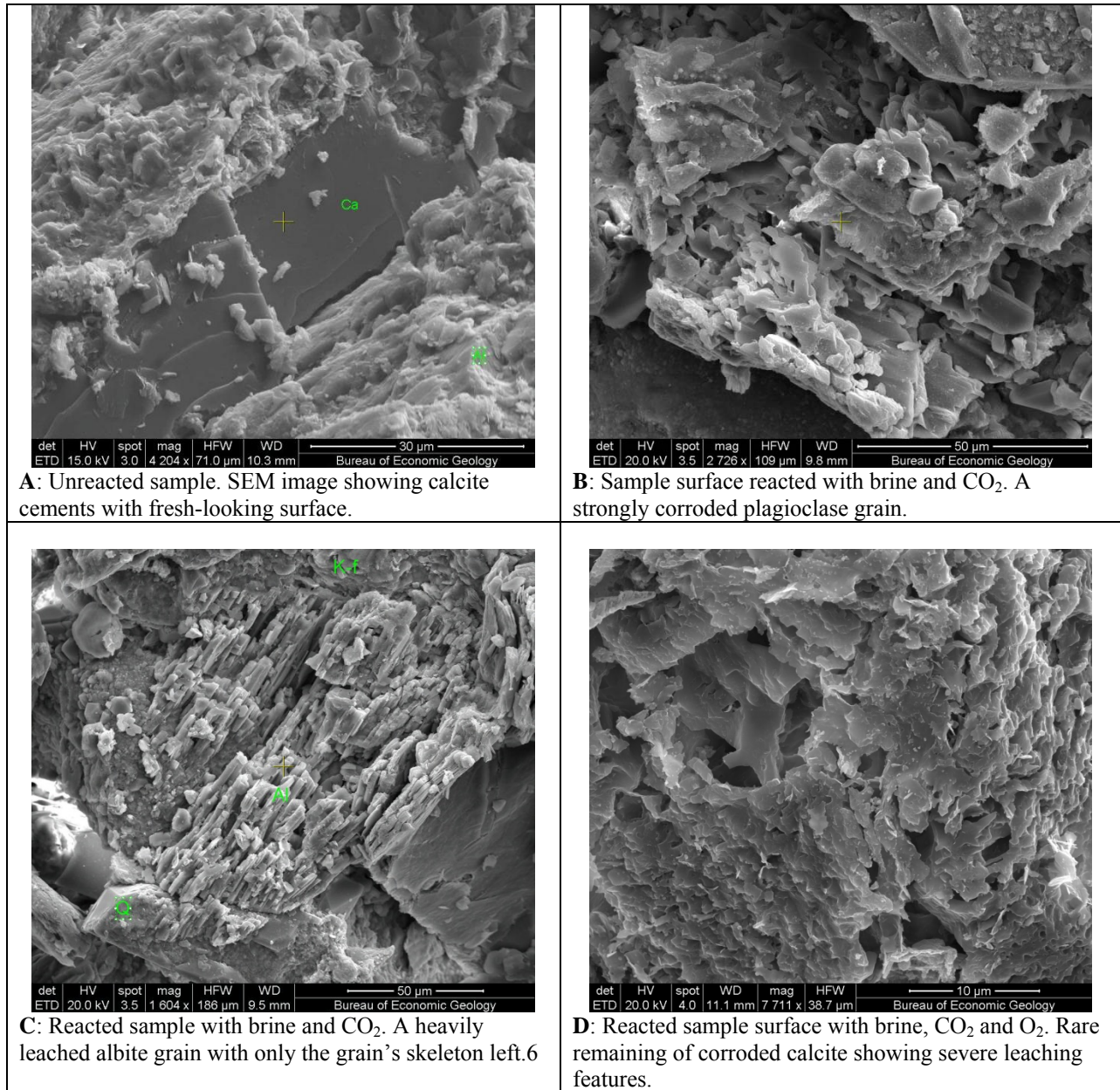


Figure 7. Unreacted and reacted Offshore Miocene samples

The Cranfield samples are fairly unreactive under pure CO₂. However, adding O₂ has a clear effect on chlorite crystals (Figure 8) which display some limited degradation dramatically expressed through a dense cover of FeOx precipitates. Very little pyrite if any is present in these Cranfield samples (as suggested also by the limited increase in sulfate concentration).

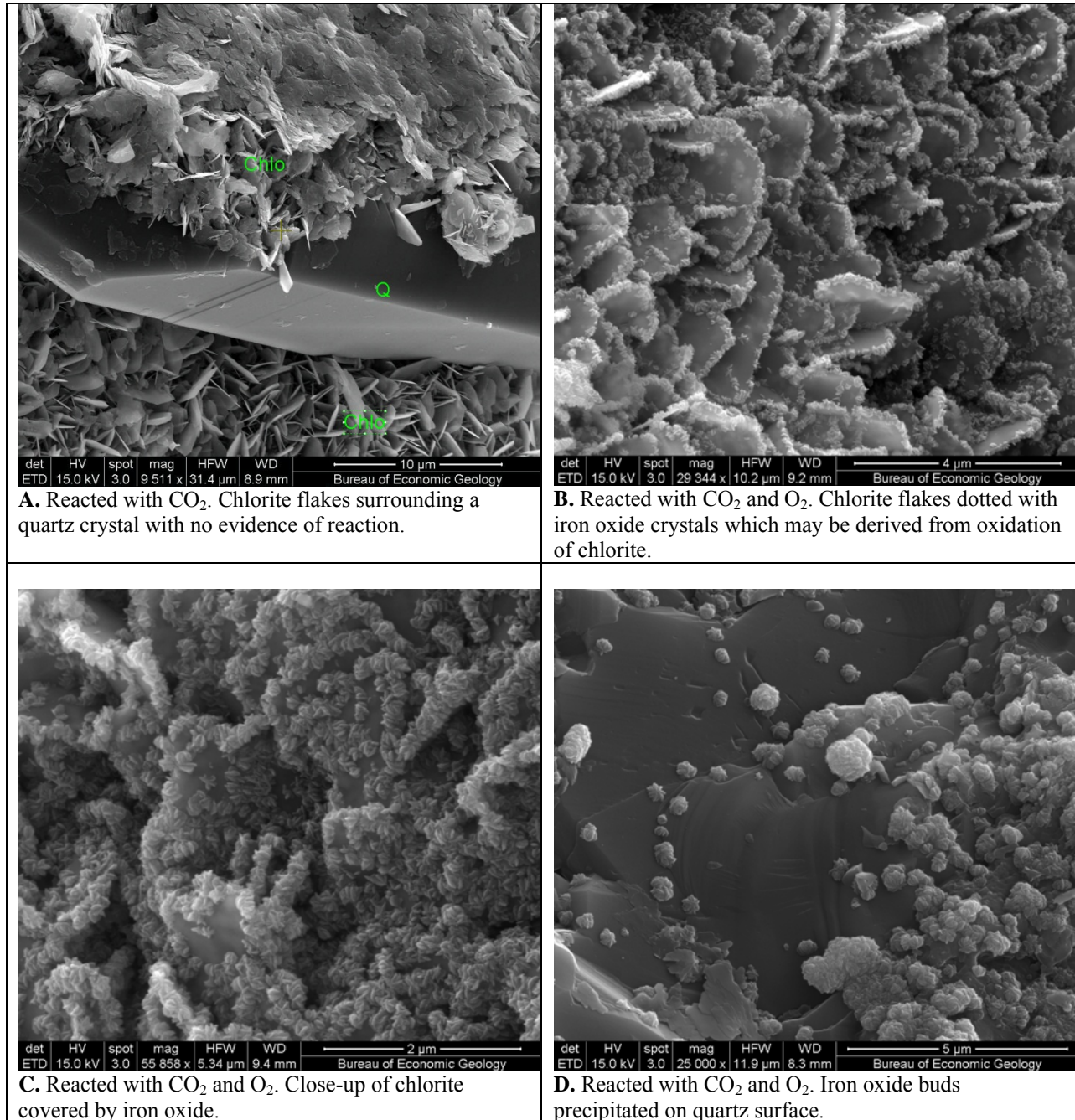


Figure 8. Unreacted and reacted Cranfield samples

The Cardium samples (Figure 9) contain two types of ferrous iron-bearing minerals: carbonates (siderite and ankerite) and pyrite. Only the latter is corroded with pure CO₂ with ferrous iron in solution. However, when O₂ is added, pyrite is also oxidized and the soluble ferrous iron is oxidized and precipitated as ferric iron-bearing FeOx minerals.

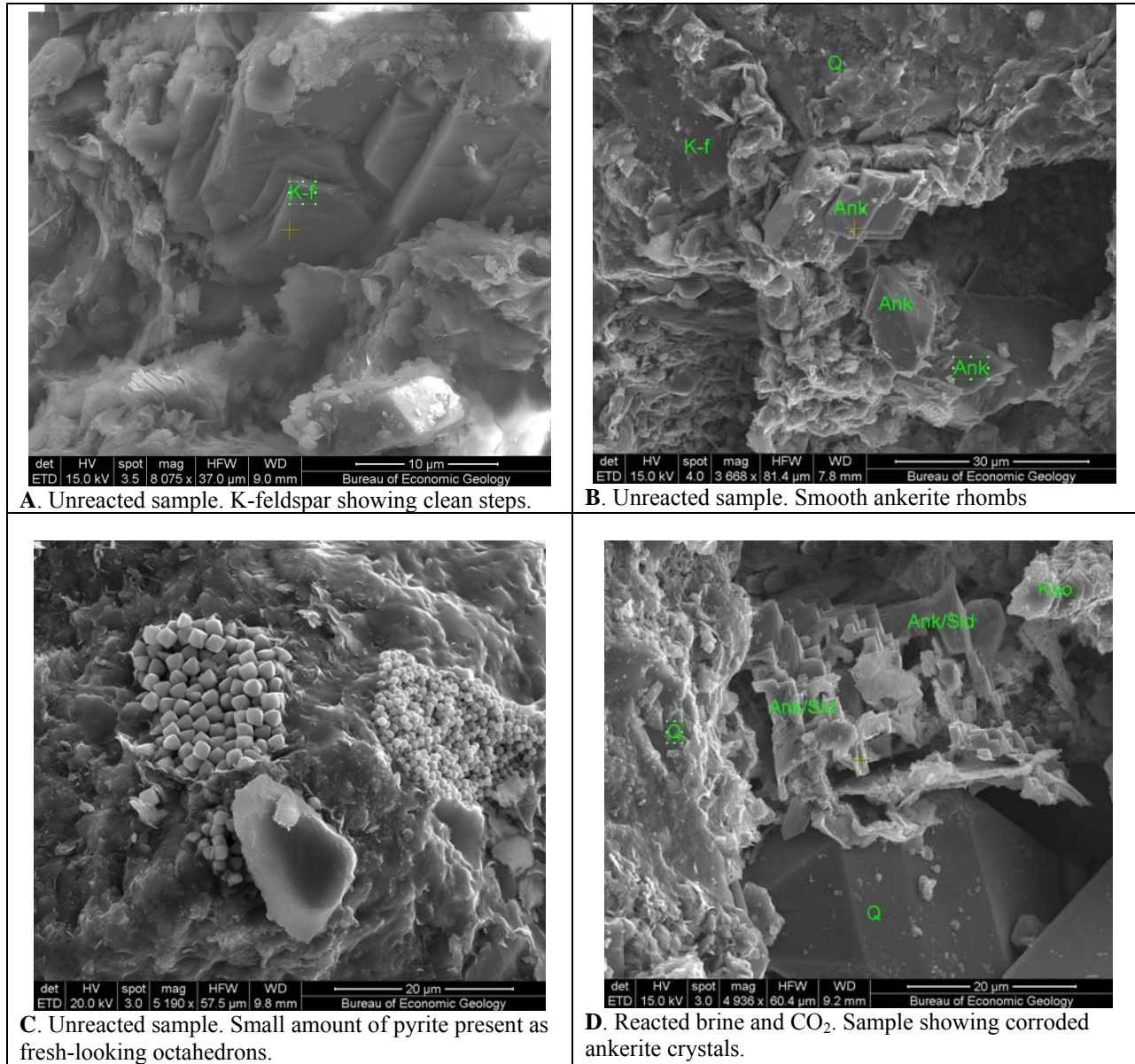


Figure 9. Unreacted and reacted Cardium samples

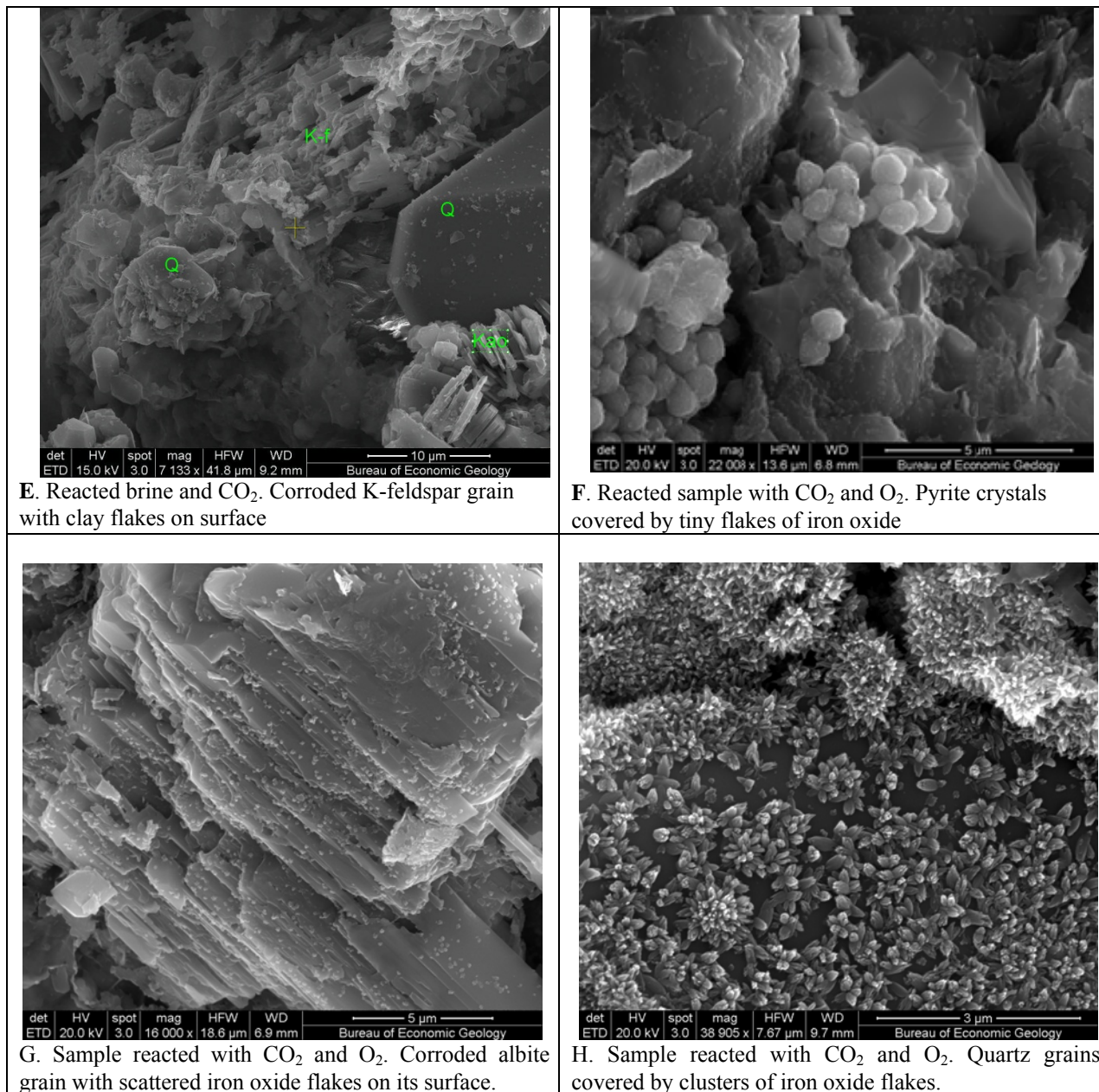


Figure 9. Unreacted and reacted Cardium samples (continued)

The analysis focuses on the differences between pure CO₂ and CO₂+O₂ mixtures systems at different temperatures. An increase in temperature, with no surprise, led to an observed increase in release rates from silicates. O₂ has an impact if there is (1) redox-sensitive mineral species and (2) ferrous iron-bearing minerals (pyrite, chlorite, siderite, ankerite, ferroan dolomite or calcite, maybe glauconite which contains mostly ferric Fe but some ferrous Fe too). The pH drop attending CO₂ injection may be mitigated or reduced by buffering species, such as carbonates or to a lesser extent through dissolution of other species such as feldspars. Once reduced species have been mobilized and are in solution, O₂ can oxidize them. A clear example is siderite or pyrite dissolution with iron hydroxides and allied species (FeOx) precipitating. Overall the release rates, although variable, are very fast with asymptotic behavior reached in a few days.

Clearly this is related to the experimental setup, columns experiments or field observations will likely reveal a much longer time frame for completion of the reactions. Batch experiments are typically rate-controlled but reactions taking place in column, and especially, field tests are generally diffusion-controlled, a much slower control.

Trace elements follow expected behavior for the most part. They are released by carbonates and feldspar dissolution (and sometimes, an experimental artifact, by reactor components exposed to O₂). Some are then sorbed by existing or newly created sorbing material such as FeOx and clays. One way to assess the importance of trace elements mobilization is to compute their concentration in a mixture of brine and mostly freshwater mimicking dilution of leaking brine in a freshwater aquifer (Table 7). The dilution has to be large to bring down the TDS of the mixture to ~1000 mg/L. Above this TDS threshold the water would not be ingested because it would be too salty. The danger would then be that a domestic well, for example, would tap water that would still meet TDS standards but lead to ingesting toxic trace metals, possibly for a long period of time. The approach followed here is to simply divide the concentration by a factor of 100. This amount of dilution would be needed to go from the ~100,000 mg/l brine to the 1,000 mg/L potable water. We compared the experimental values to EPA MCL's (<http://water.epa.gov/drink/contaminants/index.cfm>). It can be seen that oxyanion-building elements (V, Mo, Cr, As) performed better when O₂ is present. Among all elements of the table, Cr and Ni only seem to cause a problem in case of leakage but given that these elements are major components of the stainless steel reactor, their elevated presence likely results from degradation of the steel alloy. It should be noted that the resident brine may already contain some amount of trace elements that would need to be added to the amount released owing to the impact of CO₂ and impurities.

Table 7. Trace element impact

Element	Site	Pure CO ₂	O ₂ + CO ₂	Impurity lower risk?	MCL*100 (ppb)	Problem?
V	Miocene	<400ppb	<200ppb	yes	5000ppb**	no
	Cardium	<500ppb	<200ppb	yes		
	Cranfield	<200ppb	<150ppb	yes		
Cr^{^^}	Miocene	<600ppb	<1.5ppm		1000ppb	yes
	Cardium	<800ppb	<200ppb	yes		
	Cranfield	<350ppb	<100ppb	yes		
Co	Miocene	<500ppb	<300ppb			
	Cardium	<500ppb	<500ppb			
	Cranfield	<50ppb	<100ppb			
Ni^{^^}	Miocene	<15ppm	<10ppm		7ppm**	yes
	Cardium	<25ppm	<3ppm			
	Cranfield	<1ppm	<4ppm			
Cu	Miocene	<1.6ppm	<1.3ppm		150ppm	no
	Cardium	<1.5ppm	<3ppm			
	Cranfield	<1.0ppm	<3ppm			
Zn	Miocene	<800ppb	<50ppm		500ppm**	no
	Cardium	<2ppm	<30ppm			
	Cranfield	<25ppm	<15ppm			
Mo	Miocene	<3000ppb	<700ppb	yes	7000ppb**	
	Cardium	<200ppb	<150ppb	yes		
	Cranfield	<120ppb	<20ppb	yes		

Element	Site	Pure CO ₂	O ₂ + CO ₂	Impurity lower risk?	MCL*100 (ppb)	Problem?
Pb	Miocene	<80ppb	<200ppb		1500ppb	no
	Cardium	<250ppb	<500ppb			
	Cranfield	<60ppb	<50ppb			
Bi	Miocene	<1300ppb	<800ppb	yes		
	Cardium	<1000ppb	<800ppb	yes		
	Cranfield	<80ppb	<50ppb	yes		
As	Miocene	<10ppb	<5ppb		1000ppb	no
	Cardium	<10ppb	<5ppb			
	Cranfield	nd	<10ppb			
Se	Miocene	<5ppb	<10ppb		5ppm	no
	Cardium	<1ppb	<10ppb			
	Cranfield	nd	<5ppb			
Cd	Miocene	<6ppb	nd		500ppb	no
	Cardium	nd	<5ppb			
	Cranfield	nd	nd			
Sb	Miocene	<10ppb	nd		600ppb	no
	Cardium	nd	nd			
	Cranfield	nd	<2ppb			

Note: using 70°C and 3.5% O₂ data (D, R, K, N, P, O series with input for S series to correct for higher O₂ in R series; an upper limit of the long-term trend is used not necessarily the highest concentration/spike

^^: Ni and Cr concentrations are suspicious because the likelihood of steel degradation

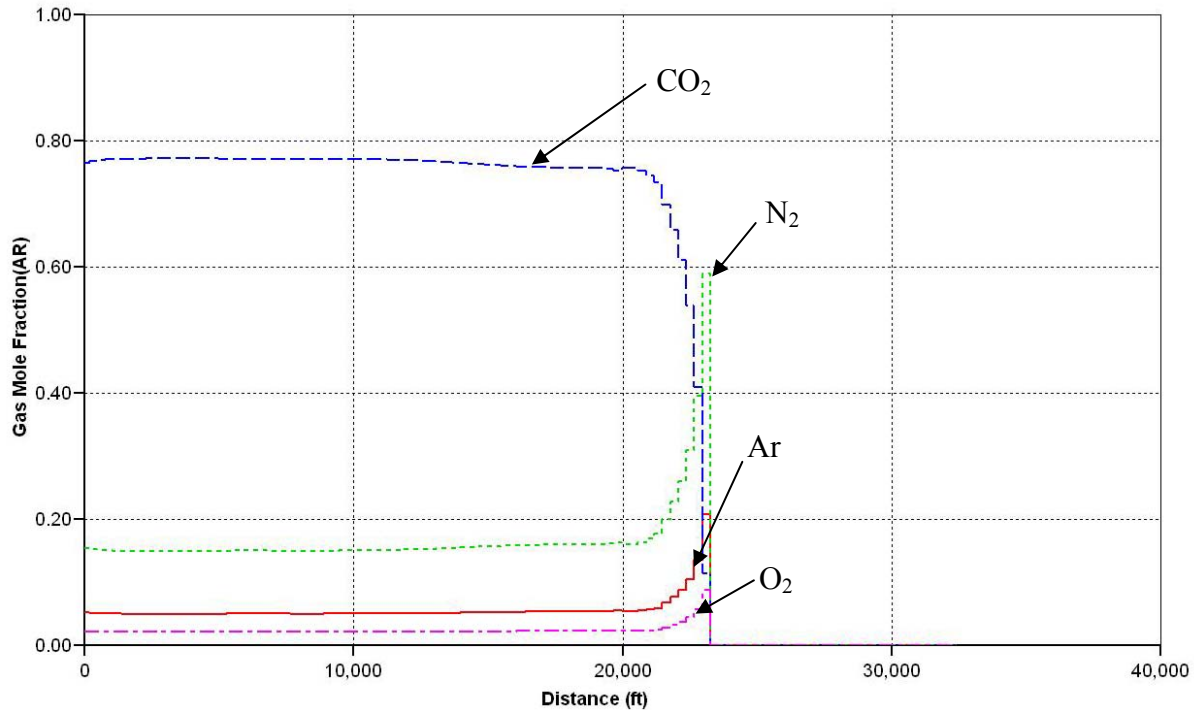
**: secondary standard only or proposed action level (state or federal) or WHO drinking water guidelines

A desktop analysis investigated the impact on CO₂ sequestration processes of trace and minor reactive acid species not dealt with in the laboratory autoclave experiments. In particular, we characterized the concentration threshold below which the species can be neglected by performing numerical geochemical simulations. Species included HCl, SO₂, NO, and NO₂ present in the waste stream of oxyfuel power plants. Results suggest that ~1000 ppm for the Frio setting (depth of ~5,000 ft, ~60°C) and ~100 ppm for the deeper Cranfield setting (depth of ~10,000 ft, ~125°C) are the threshold values beyond which the pH starts dropping significantly beyond that of CO₂ alone if no buffering capacity is available. No impact on pH was observed in the numerical experiments if buffering capacity was adequate. In the former case, trace impurities seem to have a bigger impact at depth than in shallower zones because carbonates, if present would dissolve more slowly at higher temperature. Typical concentrations of HCl and NO_x species are likely below the threshold values but SO₂ concentration is likely higher in effluent streams. When considering only the pair CO₂ + trace gas, redox conditions can also change becoming more reducing with SO₂ in the CO₂ stream and more oxidizing with NO_x. This aspect has not been studied in this work but literature exists (see Nicot et al., 2013).

To have an impact on permeability by obstructing pores, redox-sensitive minerals must be abundant enough with sufficient oxidizing material (O₂) to impact the system. A reactive transport model using the Cardium sandstones from Alberta as a test case, shows that little material precipitates compared to the pore volume (see Nicot et al., 2013). Permeability change is very sensitive to the exact location in the pore of the authigenic mineral deposits (i.e., pore throats as opposed to pore bodies) but past field experience, such as at the Rousse Field, France or injecting air or flue gas, do not point to this being a major issue.

IV. Discussion and Conclusions

The results of this study indicate that the most likely impact of non-compressible CO₂ stream impurities on clastic reservoirs will result from flow dynamics, particularly at relatively shallow depth (<4000 ft). The impact consists in longer plume extents relative to the pure CO₂ case and the additional costs it entails because of the larger Area of Review. Plume shape relative to that of pure CO₂ is more elongated along the bottom of the seal or a barrier. Similarly, because buoyant forces are larger when impurities are present, the plume or plume sections do not widen as much as in the pure CO₂ case in their rise to the top of the formation. However, increasing depth gradually reduces the impact because mixtures behave more and more like pure CO₂ due to the decreased density and viscosity contrast with neat CO₂. Reservoir rock heterogeneities tend to dampen the increased plume extent because it is distributed among several tongues (the contrast is most extreme in very simple systems). In addition, trapping occurs faster because the plume is more mobile and thus exposed to greater rock and brine volumes, affording more extensive residual trapping and, possibly, dissolution (respectively) opportunities. It will also stabilize faster. In contrast, a pure CO₂ plume travels less but stays mobile longer. However, thanks to increased mobility, the impure gas mixture may be more likely to breach a seal via enhanced buoyant pressure and a resultant leak would have to be monitored over a larger area. It also suggests a trade-off between plume extent (area of review) and decreased long-term risk owing to faster trapping. In addition, because of differential solubility, the front and edges of the plume will be enriched in impurities owing to higher CO₂ solubility under all subsurface conditions (Figure 10). Note that the figure was constructed assuming non-reactive gases; O₂ is likely to be consumed faster than it can becomes enriched at the plume edge.

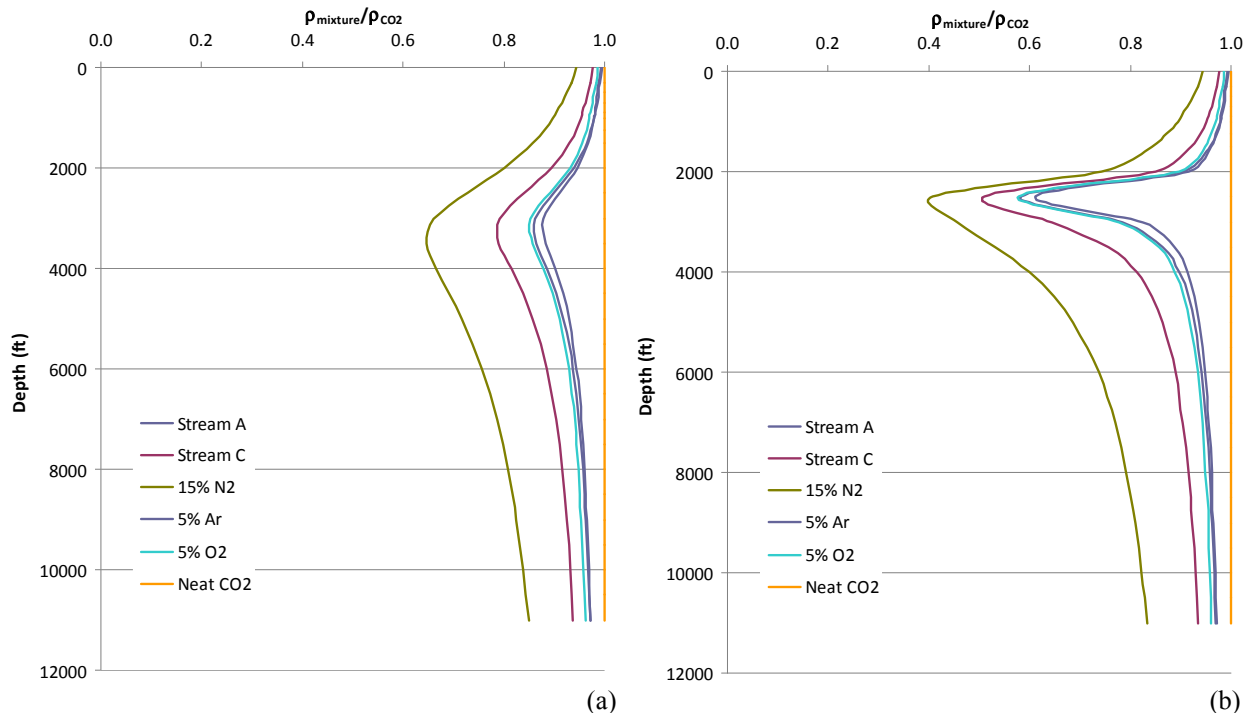


Note: generic model, 100 years after start of injection; ~78% CO₂, 15% N₂, 5% Ar, and 2% O₂ mole fraction; profile along the main axis of the plume. Tuned solubility models are used (see Nicot and Solano, 2012).

Figure 10. Impact of dissolution at gas composition at plume front

In terms of trapping, we discussed hydrodynamic trapping above (faster than with pure CO₂ but potentially occurring farther away from the injection well(s)). In the course of the study, we neglected any impact on interfacial tension and any subsequent change on pressure. IEAGHG (2011) cites references suggesting that the interfacial tension (IFT) of a CO₂ mixture with N₂ or O₂ is higher than that of neat CO₂, likely increasing the maximum residual saturation and perhaps balancing the decrease in residual phase density along with CO₂ mole fraction. Impact of alteration of mineral surface area (degradation of minerals, creation of new surfaces) on wettability, relative permeability, and ultimately residual saturation is unknown. Addition of a small amount of impurities is unlikely to change long-term fate of CO₂ under the solubility and mineral trapping modes.

We addressed capacity of structural traps by comparing density of net CO₂ vs. density of CO₂-rich mixtures as a function of depth (Nicot and Solano, 2012). The impact on capacity (with density ratio of mixture to neat CO₂ as a proxy) is a strong function of the geothermal and pressure gradient. For reasonably low and high geothermal gradient, density ratio plots show a large drop in capacity around 3000 ft, which is slightly below the accepted depth to keep CO₂ stream in a supercritical state. In other words, the impact of impurities on storage capacity decreases with increasing depth (Figure 11). The effect is the largest for the lower geothermal gradient (only 40% of neat CO₂ capacity at shallow depth) because the density contrast between neat CO₂ and mixture is more pronounced in that case. A more systematic way of addressing structural trapping capacity changes would be, for example, to build a numerical model with a structural trap and a spill point and compute the maximum amount of CO₂ stored before it leaks in various combinations of depth, geothermal gradient, and mixture composition.



Note: Pressure gradient is 0.465 psi/ft (all) and geothermal gradient is 18°F/1000ft (a) or 10°F/1000ft (b).

Figure 11. Mixture density relative to neat CO₂ as a function of depth.

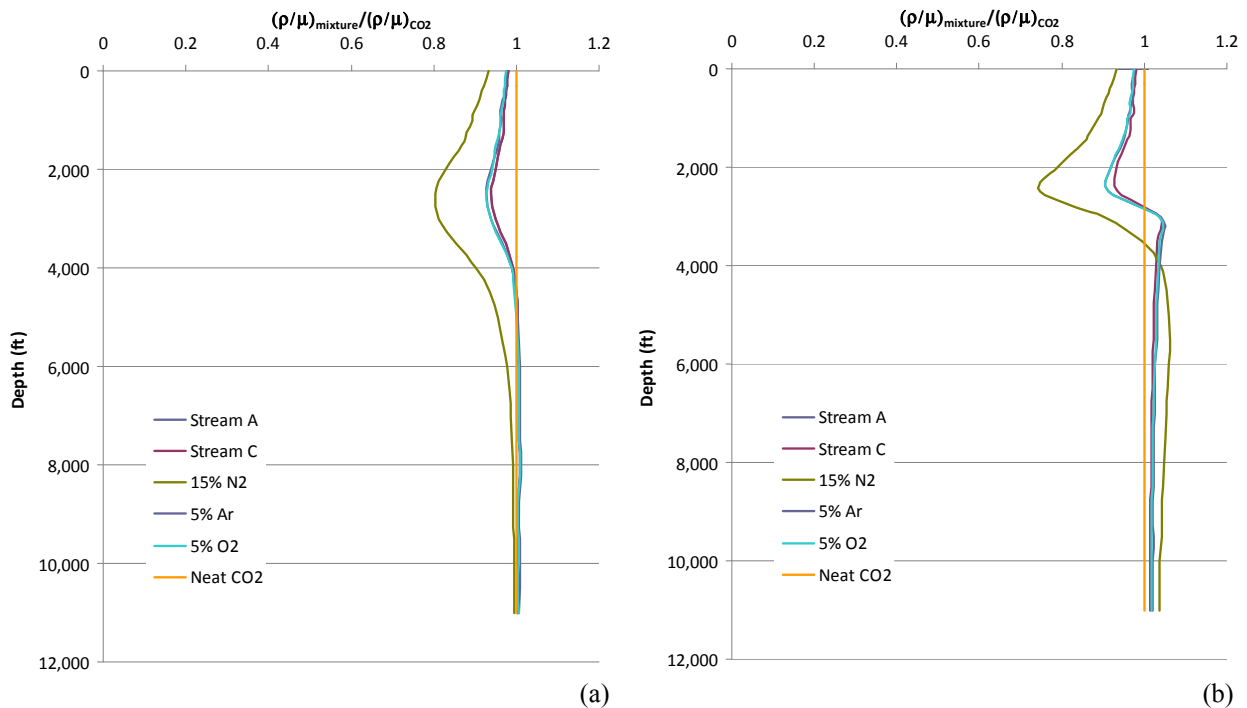
The impact of impurities on well injectivity can be analyzed the following way; injectivity J is usually defined as the ratio of flow rate over pressure drop at the wellbore:

$$J = \frac{q}{P_{wf} - P_a}$$

where q is injection rate and p_{wf} and p_a are bottomhole flowing pressure and reservoir-averaged pressure. We assume that there is no water alternating gas (WAG) and that a continuous gas stream is injected, limiting the relative permeability effects. The injection rate q_v is expressed by the commonly-used extension of Darcy's law to multiphase flow which combined with the conservation of mass equation yields:

$$q_v = \frac{4\pi kb\Delta P}{\mu} \left[\ln \left(\frac{2.25kt}{\phi c \mu r^2} \right) \right]^{-1}$$

where c is the compressibility of the fluid. Note that c intervenes within a log term mitigating any impacts of its variations on injectivity compared to viscosity. Compressibility value variations and reveals that they stay within a factor of 2 or 3 for the various mixtures numerically tested (Nicot and Solano, 2012, Appendix B). An approximate metric of injectivity change is then the ratio of the inverse of the viscosities. An alternate definition of injectivity is defined not in terms of volume flux q_v , but in terms of mass flux q_m , $q_m = \rho q_v$ of CO₂ and impurities injected. In this case, an approximate metric of injectivity change is the ratio of the density-viscosity ratios. There is a general increase in viscosity and density with depth but that of mixtures is in most conditions lower than that of pure CO₂. Figure 12, based on the ratio of the density over viscosity ratios, suggests that mass rate injectivity is not much affected by impurities except at relatively shallow depths at which it may show a decrease by a maximum of approximately 20% and <10% in most likely compositions (streams A and C).



Note: Pressure gradient is 0.465 psi/ft (all) and geothermal gradient is 18°F/1000ft (a) or 10°F/1000ft (b).

Figure 12. Mixture density-viscosity ratio relative to that of neat CO₂.

Impurities may have a small positive effect by increasing mass flow rate at locations with a low geothermal gradient. This result assumes thermal equilibrium between the CO₂ stream and the formation which, depending on the flow rate, is not necessarily the case.

Reservoir storage integrity could be impacted if impurities (1) negatively affect the capillary barrier mechanism holding the gas phase in the injection interval or (2) promote permeability of the confining system. An increase in IFT, as it seems would happen with common impurities (N₂, Ar, and O₂), would reinforce the capillary barrier effect making the reservoir more secure if it increases faster than the balancing force due to increased buoyancy. Overall permeability changes resulting from interaction of the seal minerals with reactive gases (mainly O₂) are unclear. On the one hand, precipitation of FeOx may decrease permeability but, on the other hand, oxidation of pyrite, common in shales, a typical seal, may generate a lower pH than with pure CO₂, dissolving carbonates more thoroughly and altering clays in a detrimental way. Although speculative until column experiments are done, it appears that reactive gases would be consumed largely before the whole thickness of the confining system is impacted. On the rare instance leakage will occur, either because of the presence of impurities or more likely for some unrelated cause, the impacts on underground sources of drinking water (USDW) can be binned into two groups as done in many publications: (1) impact of a leaking gas phase and (2) impact of a leaking brine in equilibrium with the CO₂-dominated mixture. We did not investigate the former but O₂, if not consumed at depth, would have similar action on aquifer material, generally at reducing conditions at the lower limit of the USDW and could mobilize EPA-regulated elements. On the other hand, Table 7 suggests that, when diluted to drinking water standards and in the case of the three clastic aquifers studied, a leaking brine would not bring enough regulated elements or chemical species to endanger health and safety.

Many aspects of impure CO₂ streams remain to be investigated. Because the results depend on viscosity and density models, their sensitivity must be tested with alternate EOS and formulations of the flow parameters. Impact of IFT and wettability changes due to impurities on residual saturation and relative permeability curves also need to be examined. The scope of flow dynamics sensitivity analysis can be further extended to include various formation dip angles, anisotropy ratio, and closed boundary conditions. Other relevant exercises such as monitoring leakage through a (leaking) well located at some distance from the injection well as a function of injection-stream composition could also be performed. Geochemical impacts need to be tested with more reservoir rock types, in particular carbonate rocks. Although batch experiments are very informative, column experiments are needed to better understand potential permeability changes and assess the actual release and reaction rates. Investigative studies of geochemical impact on seals are also needed. Because they are easier to perform and do not require an autoclave reactor, some studies on impact of impurities on aquifer material have already been performed, although not necessarily in the geological sequestration context. Laboratory experiments should be preceded by a thorough collection of previous results.

V. References

- IEAGHG, 2011, Effects of Impurities on Geological Storage of CO₂, report 2011/04 prepared by CanmetENERGY, Natural Resources Canada, June, 63 pages + Appendices.
- Nicot, J. -P., and Solano, S. V., 2012, Impact of CO₂ impurities on storage performance and assurance; Tasks 1 and 2: Plume dynamics: The University of Texas at Austin, Bureau of Economic Geology, contract report prepared for CO₂ Capture Project Phase III (CCP3), 155 p.
- Nicot, J.-P., J. Lu, P. Mickler, C. Yang, K. Romanak, and T. Zhang, 2013, Impact of CO₂ impurities on storage performance and assurance; Tasks 3 and 4: Geochemistry: The University of Texas at Austin, Bureau of Economic Geology, contract report prepared for CO₂ Capture Project Phase III (CCP3), 224 p.
- Thibeau, S., and A. Dutin, 2012, Large scale CO₂ storage in unstructured aquifers: Modeling study of the ultimate CO₂ migration distance, 11th International Conference on Greenhouse Gas Control Technologies (GHGT11), International Energy Agency Greenhouse Gas R&D programme, Kyoto, Japan, November 18–22, 2012, 8p.
- Wang, J., 2011, D. Ryan, E. J. Anthony, N. Wildgust, and T. Aiken, Effects of impurities on CO₂ transport, injection and storage, Energy Procedia, Vol.4, p. 3071-3078.

